

Extending the Current Collector into the Nanoporous Matrix of Dye Sensitized Electrodes

Shlomit Chappel, Larissa Grinis, Ashi Ofir, and Arie Zaban*

Department of Chemistry, Bar-Ilan University, Ramat-Gan 52900, Israel

Received: November 4, 2004; In Final Form: December 23, 2004

A new type of high surface area TiO_2 electrode for DSSCs is proposed. The new electrode consists of a transparent conductive nanoporous matrix that is coated with a thin layer of TiO_2 . This design ensures a distance of several nanometers between the TiO_2 –electrolyte interface and the current collector throughout the nanoporous electrode, in contrast to several micrometers associated with the standard electrode. In addition the new electrode contains inherent screening capability due to the high doping level of the conducting core matrix. Theoretically, this electrode should overcome the collection and image field problems associated with solid-state DSSCs. Using a flat analogue of the new electrode we show that unless the TiO_2 coating is thicker than 6 nm, the electrode performance is very low due to fast recombination. Two mechanisms for the thickness effect on the recombination rate, that are proposed, provide new insight to the DSSC operation.

Introduction

Efficient light-to-energy conversion of dye-sensitized solar cells (DSSCs) requires that the sensitized semiconductor electrode will have a high surface area. The high surface area is necessary because of the low absorbance of dye monolayers and the low efficiency of dye multilayers.¹ Various high surface area electrodes of wide band gap semiconductors were tested in DSSCs. The common electrodes are made by the deposition of a nanosize semiconductor layer on a transparent current collector yielding a porous geometry.² The most common wide band gap semiconductors in DSSC studies and applications is the TiO_2 which was presented in the first report of efficient DSSC.³ Other materials such as SnO_2 , ZnO , Nb_2O_5 , and SrTiO_3 were found to be less efficient than the TiO_2 .^{1,4,5}

A schematic view of the charge transport in the volume of a standard nanoporous electrode during the DSSC operation is shown in Figure 1. One can clearly see the two main problem associated with the porous geometry: (a) the high area cross-section for recombination of the photoinjected electron with the holes that are transferred to the electrochemical mediator and (b) the image field opposing the separation process that is distributed inside the nanoporous electrode. The recombination process has been the subject of many studies yielding various methods to minimize this loss path. The most recent approach involves nanoporous electrodes in a well-defined core–shell configuration, mainly TiO_2 core coated with Al_2O_3 , MgO , or Nb_2O_5 .^{6–9} The shell having a more negative conduction band potential acts as an energy barrier that slows recombination reactions. However, there is still considerable recombination that increases with the distance between the electron injection point and the current collector. In other words, the limited lifetime of the injected electron and the slow diffusion rate inside the porous structure limit the effective thickness of the nano-

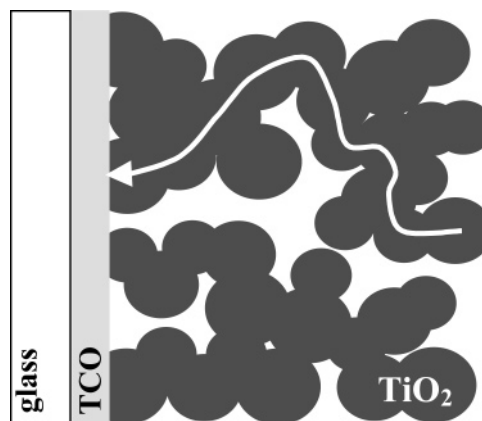


Figure 1. Schematic view of the charge transport in the volume of a standard nanoporous electrode during the DSSC operation.

porous electrode. The image field has been discussed intensively in several publications, showing that high doping of either the semiconductor or the electrochemical mediator can screen this field.^{10–13} For this reason, the electrolyte based cells that contain positive counterions capable of screening the electrons from their image holes are more efficient than the solid state cells. Methods to overcome this problem usually involve the addition of moving ions to the solid mediator, which in most cases involve the addition of the undesired electrolyte.

For several years, we have been trying to develop a new high surface area electrode that can overcome both the recombination and image field problems, aiming at a generic substrate for efficient solid state DSSCs. The new electrode design, shown in Figure 2a, involves a core shell configuration. However, in contrast to the previous design, the new electrode is based on a conductive nanoporous core rather than a semiconducting one. Consequently the electrode consists of a conductive nanoporous matrix that is coated with a standard DSSC wide band gap material. To maintain transparency of the electrode, the inner

* Corresponding author. Telephone: 972-3-5317876. E-mail: zaban@mail.biu.ac.il.

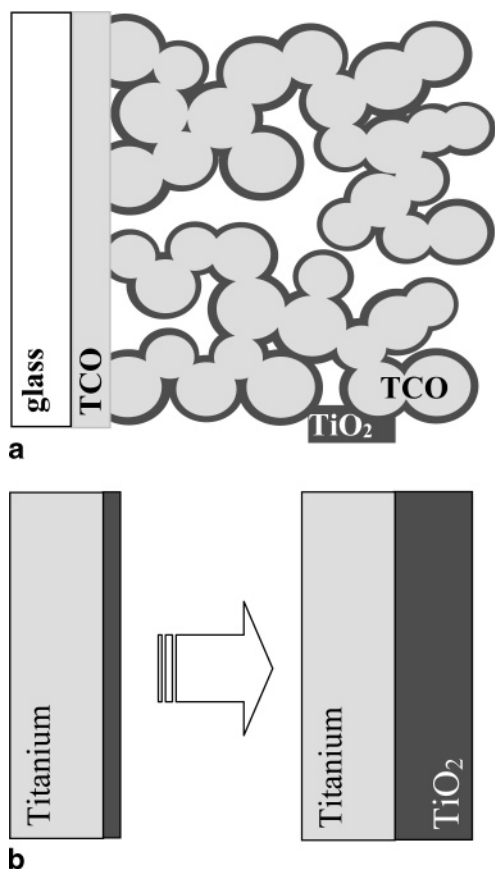


Figure 2. (a) Schematic view of the collector-shell electrode. This core shell electrode consists of a conductive nanoporous matrix that is coated with a standard DSSC wide band gap material (typically TiO_2). (b) Flat analogue of the nanoporous collector-shell electrode presented in part a. Here the conductive titanium collector is coated with TiO_2 .

core matrix was made from nanocrystals of ITO or Sb doped SnO_2 and the shell consisted of TiO_2 . In principle, the conducting core extends the current collector into the nanoporous network and is thus denoted the nanoporous "collector-shell electrode". Consequently the distance between the injection spot and the current collector should decrease to several nanometers throughout the nanoporous electrode, in contrast to several micrometers associated with the standard electrode. In other words, all electrons injected into the electrode, including those that are generated several micrometers away from the substrate, have to travel a very short distance before reaching the current collector. As shown by several studies, transport that is shorter than $1 \mu\text{m}$ provides 100% collection efficiency.¹⁴ In addition the new collector-shell electrode contains inherent screening capability due to the high doping level of the conducting matrix. Theoretically the new design should enable efficient charge separation and collection for thick nanoporous layers and solid electrochemical mediators.

Despite our intensive activity resulting in collector-shell electrodes of several material combination, the performance measured in DSSCs was quite low. We note that the low performance in DSSCs is not related to coating discontinuity as confirmed by several electrochemical measurements.¹⁵ At this point, we decided to examine the effect of the shell thickness on the electrode performance in DSSC, a correlation that has never been tested. Using a flat analogue of this core shell system, we report here results that indicate optimal thickness for the shell material and some insight into the DSSC mechanism.

Experimental Section

Electrode Preparation. All electrodes used in this work were fabricated using a titanium plate (99.7% purity, Alfa Aesar). Each Ti sample (approximately $1.5 \times 2 \times 0.09 \text{ cm}^3$) was polished by silicon carbide papers of increasing smoothness followed by an alumina paste, resulting in bright appearance. Chemical etching followed the mechanical polish; the metal sheets were dipped in three different solutions:¹⁶ (1) HF (185–200 g/L) and HNO_3 (10–15 g/L), dip for 15–20 s and then rinse with water; (2) HF (350–400 g/L) and HNO_3 (20–30 g/L), dip for 15–30 s and then rinse with water; (3) 5% potassium sodium tartrate tetrahydrate and water. The quality of the resulting Ti surface determined the quality of the results mainly with respect to the thickness measurement.

Surface oxidation to TiO_2 . Two oxidation procedures were used in this study:

(1) **Thermal Oxidation.** The etched titanium sheets were heated in air for 1 h in an electric furnace to temperatures between 300 and 1000 °C. The thickness of the oxide layer obtained depended on the heating temperature.

(2) **Anodic Oxidation.** An electrochemical method was used to produce metal oxide films on a metal surface. The oxidation was performed in a two-electrode cell using a Ti anode, and a platinum foil as a cathode. For electrolyte an aqueous solution of trisodium phosphate (10% in deionized water) was used.¹⁷ A constant current of 1 mA was applied to the system by an Ecochemie Autolab 30 Potentiostat, for different time periods. The process duration provided a series of thin layer TiO_2 electrodes. Only a specific area of 2.5 cm^2 of the film was exposed to the solution, limited by an O-ring. After the oxidation process the films were rinsed with deionized water to remove the trisodium phosphate. In some cases heat treatment of 400 °C for 20 min. was added to improve the crystallinity of the TiO_2 .

Electrochemical Impedance Spectroscopy Measurements. EIS measurements (1 kHz to 1 Hz) were made by an Ecochemie Autolab 30 Potentiostat. Zview software (Scribner Associates) was used to model the impedance spectra. The electrochemical experiments were performed in a three electrodes cell: WE, Ti/ TiO_2 electrode; RE, Ag/AgCl; CE, Pt. The electrolyte consisted of 0.2 M LiClO_4 in acid (pH 1.8 HClO_4). In this cell, the TiO_2 electrode was pressed against an O-ring to define its geometrical surface area. An equivalent electrical circuit containing a constant phase element (CPE) in parallel with R_p , both in series with a solution resistor (R_s), was used to fit the spectra and calculate the TiO_2 thickness.

Solar Cell Measurements. The Ti/ TiO_2 electrodes were sensitized by the N3 dye [*cis*-di(isothiocyanato)-*N*-bis(2,2'-bipyridine-4,4'-dicarboxy)ruthenium(II)] (Solaronix SA). Dye adsorption to the electrodes was done by overnight immersion in a 0.5 mM ethanolic solution of the dye. The solar cell electrolyte solution consisted of 0.5M TBAI (tetrabutylammonium iodine)/0.05M I_2 in 1:1 acetonitrile: NMO (3-methyl-2-oxazolidinone). The electrode illumination, with a 150 W Xe lamp, was done from the counter electrode side using a homemade electrochemical cell that ensures similar electrolyte layer thickness in all measurements. Consequently all electrodes experienced the same illumination intensity.

For the V_{oc} decay measurements the cell was illuminated to a steady voltage. The illumination was turned off using a shutter. Placing neutral density filters in the illumination path performed a systematic change of initial steady state conditions. The open circuit photovoltage decay was recorded using an Ecochemie potentiostat equipped with a short interval sampling module.

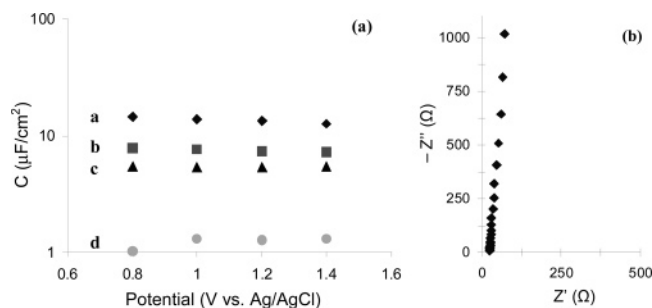


Figure 3. (a) Typical electrochemical impedance spectroscopy (EIS) results for a standard set of electrodes that vary by the thermal oxidation temperature: (a) 300, (b) 400, (c) 500, and (d) 600 °C. At positive potentials the calculated capacitances of each film is constant. The variation between films indicates the different thicknesses of the TiO_2 layer. (b) Typical Nyquist EIS plot from which the TiO_2 capacitance (and thickness) was calculated. WE = Ti/TiO_2 , RE = Ag/AgCl , CE = Pt, and electrolyte = 0.2 M LiClO_4 in acid (pH 1.8 HClO_4).

Typically the measurement interval was 10–50 ms. The V_{oc} decay analysis refers only to values measured after the shutter obtained full darkness.

Results and Discussion

A schematic view of the collector–shell electrode and its flat analogue are shown in Figure 2 (parts a and b, respectively). The flat analogue consists of a titanium foil whose surface is oxidized to TiO_2 by several methods. This choice of material ensures that, even for very thin TiO_2 layers, full coverage of the current collector (the Ti metal) with the oxide layer is achieved; i.e., no pinholes are present in the electrode. The TiO_2 layer was formed by several methods that are well established in the literature. Generally the results were independent of the electrode fabrication method. We therefore concentrate on two procedures that enabled high resolution with respect to the TiO_2 thickness, as well as good reproducibility. The first method involved thermal oxidation in air.^{18,19} The temperature and the duration of the oxidation process were used to determine the thickness of the TiO_2 layer. The second method was based on electrochemical oxidation.^{20,17} Here the applied potential and the oxidation duration were the thickness controlling parameters. The electrochemical oxidation was followed by a heat treatment which typically improves the crystallinity of TiO_2 .

The thickness of the TiO_2 layer was measured by electrochemical impedance in the potential range of +1.4 to -0.8 V vs Ag/AgCl . This potential range is located deep in the TiO_2 band gap thus a pure TiO_2 layer should generate an interfacial capacitance.²¹ Electrochemical impedance spectroscopy (EIS) is the optimal tool for the measurement of thin layer capacitance, since the issue of contacts is inherently solved by the electrolyte. Moreover EIS provides information regarding the uniformity of the surface, mainly with respect to the surface roughness, which results in a distribution of the interface time constants.

Figure 3a shows typical EIS results for a standard set of electrodes characterized by different oxidation temperatures. A typical Nyquist impedance plot, shown in Figure 3b, reflects an almost perfect capacitor with a small distribution of its time constant. Thus results are presented in the form of calculated capacitance, using a simple constant phase element (CPE)^{22–24} to fit the impedance spectra. Since the effective surface area of the electrode plays a major role in the calculation of the insulating layer (TiO_2) thickness, only electrodes that exhibit a CPE power that is higher than 0.92, were further evaluated. The thickness of the TiO_2 layer was calculated using the parallel-plates capacitor equation ($C = \epsilon_0 \epsilon A/d$)²² using $\epsilon = 50$.²⁴ We

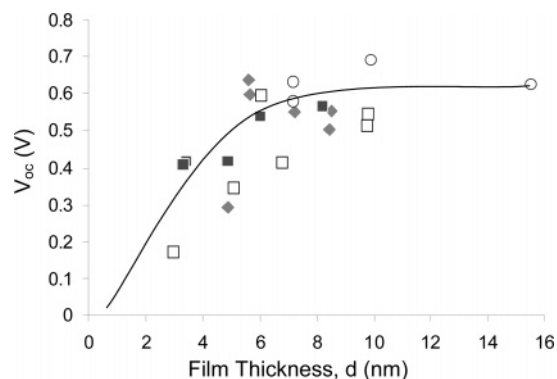


Figure 4. Correlation between the thickness of the TiO_2 layer and the open circuit photovoltage in the DSSC. The symbols represent sets of electrodes that were made by the different preparation methods of the compact TiO_2 . The solid line is added to highlight the general trend.

note that the measured capacitances are smaller than the double layer capacitance of a Pt electrode in the same electrolyte and potential range. This ensures that out of the two series capacitors, the double layer and the insulating TiO_2 , the latter is measured.

Following the evaluation of the compact TiO_2 layer thickness, the electrodes were coated with the N3 dye and tested in a solar cell. The cell illumination was limited to 470–750 nm to ensure that no direct contribution of the TiO_2 is measured. The illumination procedure (see Experimental Section) ensured that all the electrodes experienced similar illumination intensity. The low viable range absorbance of the cells, which consists of a compact TiO_2 layer, imposes very low photocurrents. Thus the discussion will focus on the photovoltage based analysis of the system.

Figure 4 shows the correlation between the thickness of the TiO_2 layer and the open circuit photovoltage, V_{oc} , of these DSSCs. The symbols represent the different preparation methods of the compact TiO_2 while the solid line is added to highlight the general trend. Figure 4 shows that the V_{oc} is basically constant once the compact TiO_2 layers are thicker than 6 nm (data available up to 16 nm). In contrast, layers that are thinner than ca. 6 nm impose significant decrease of the V_{oc} , as the films are made thinner. In the remaining of the paper we discuss the results presented in Figure 4 suggesting two alternative mechanisms. However we would first like to emphasize the practical implication of the results mainly with respect to the collector–shell electrode.

Most of the reported core–shell electrodes, including those that consist of conductive core (i.e. variations of the collector–shell electrode), were made by dip coating.^{15,25,7} Typically this procedure yields a shell with a thickness ranging between 0.5 and 2 nm. Consequently, a collector–shell electrode that is made by dip coating is too thin to establish reasonable V_{oc} (or photocurrent as will be shown below). The results presented in Figure 4 are therefore very important from the practical point of view. They not only explain the fact that an efficient collector–shell electrode has not been produced so far, but, also, lead us to the conclusion that in order to achieve this goal, a semiconductor shell thicker than 6 nm must be fabricated. Research in this direction is currently underway but is complicated by the effect of such a thick coating on the porosity of the electrode.

Figure 5a presents the V_{oc} decay curves of six DSSCs containing a series of Ti/TiO_2 electrodes that differ by the thickness of the compact TiO_2 layer (3–16 nm). The V_{oc} decay technique relates to monitoring of the open circuit voltage of illuminated cell, starting the moment the illumination is turned

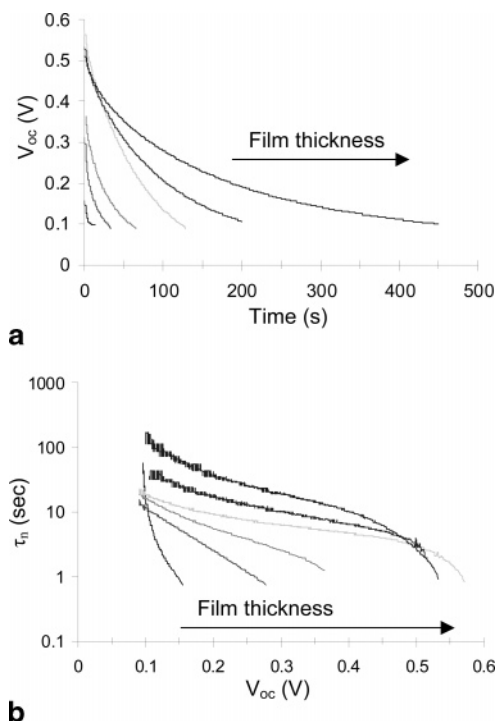


Figure 5. (a) V_{oc} decay curves of six DSSCs containing a series of Ti/TiO₂ electrodes that differ by the thickness of the compact layer. (b) Electron lifetime (τ_n) as a function of the cell voltage, calculated for the six V_{oc} decay curves presented in part a. The correlation between τ_n and the cell voltage is highly dependent on the thickness of the TiO₂ layer up to 6 nm.

off. In other words V_{oc} decay is a dark measurement of the DSSC that utilizes the steady-state V_{oc} of the illuminated cell as the starting potential. Detailed description of the technique is provided in previous publications²⁶ where it is shown that the electron lifetime in the TiO₂ electrode can be calculated from the voltage decay data, starting at V_{oc} down to ca. 100 mV above the dark equilibrium potential. Consequently, one can plot very detailed curves of the correlation between the electron lifetime in the TiO₂ electrode, τ_n , and the cell potential.

Figure 5b presents the calculated τ_n vs the cell's voltage showing that the electrode thickness has a significant influence on τ_n throughout the potential range. The lifetime is calculated with the expression²⁶

$$\tau_n = -\frac{k_B T}{e} \left(\frac{dV_{oc}}{dt} \right)^{-1} \quad (1)$$

This equation is strictly valid for mesoporous TiO₂, where the electron density and the recombination are homogeneous in the film. In the present case the recombination occurs at the outer surface only, and it pulls down the Fermi level during the decay, restoring the bandbending. Therefore in the case of the thin film eq 1 provides an estimation of the electron lifetime, although a more accurate expression requires a complete model for the electron distribution in the film, according to the situations that will be discussed later. Here we discuss the rate of recombination using eq 1 as a phenomenological expression.

As the thickness of the TiO₂ layer increases, the $\tau_n(V)$ curves become less steep resulting in slower recombination rates per a given voltage (V_{oc}). The significant thickness dependence of the electron lifetime is mainly associated with the thin electrodes. Once the TiO₂ layer thickness crosses ca. 6 nm, the difference between the $\tau_n(V)$ curves especially at the high voltage region becomes small. These results correlate well with the data

presented in Figure 4, which shows the dependence of the achieved V_{oc} on the thickness of the TiO₂ layer up to 6 nm, where the maximum value is achieved. We therefore conclude that the correlation presented in Figure 4 is a result of the increasing recombination rate, associated with a decrease of the TiO₂ thickness once this layer is thinner than 6 nm.

The dependence of the $\tau_n(V)$ curves on the electrode thickness can be understood by two alternative mechanisms that focus on either the photoinjected electron or on the hosting TiO₂.

The first approach views the change in recombination rate as a gradual change that is associated with the distance of the electrons from the TiO₂ surface. According to this mechanism, the TiO₂ layer consists of two regions:²⁷ (i) the recombination region close to the TiO₂–electrolyte interface (assuming tunneling in the first few nanometers) and (ii) an inner part that necessitates electron transport to the electrode–electrolyte interface prior to recombination. The electron transport results in a slower reaction rate that depends on the electron density in the TiO₂, i.e., the V_{oc} . In thin films, only the recombination region is available while thick films consist of both the recombination and the inner parts. Thus, the results presented in Figures 4 and 5 reflect a change in the rate-determining factor of the recombination process from surface reaction control, in the thin films, to transport limited rate in the thick ones. In this mechanism the gradual slowing of the recombination for a given V_{oc} , is associated with an increase of the number of electrons present in the inner part in comparison with the number present in the recombination region. Above a thickness of 6 nm the transport rate dominates the overall recombination rate.

The second mechanism relates the change in recombination rate with the nature of the TiO₂ layer. According to this approach, the layer reaches the standard TiO₂ properties only when thicker than 6 nm. Thinner layers, despite having the anatase TiO₂ structure, are affected by the two interfaces with the electrolyte and the Ti metal, resulting in a material that is not as efficient as standard TiO₂ for DSSCs. Consequently the results presented in Figures 4 and 5 reflect properties changes in the whole TiO₂ layer until a constant material is achieved at 6 nm.

Conclusions

In this paper, we present a concept for a new nanoporous electrode for DSSCs, the collector–shell electrode. This electrode is expected to be more efficient than the standard electrodes, especially in the case of solid-state systems that lack ionic screening. Using a flat analogue of the collector–shell electrode we examined the shell thickness influence on the DSSC properties. We find that the V_{oc} increases with the shell thickness up to ca. 6 nm where a plateau is measured. Practically, the results indicate that the collector–shell electrode will become efficient only once a way is found to fabricate a 6 nm shell. However, with the V_{oc} decay method, the flat system seems to provide new insight into the DSSC operation by the ability to separate the surface recombination rate and the rate of electron transport from the inner part of the TiO₂ to the electrode surface. New methods to fabricate an efficient collector–shell electrode currently being developed will be reported when successfully achieved.

Acknowledgment. The authors thank the Israel Ministry of Infrastructures for the support of this work.

References and Notes

- (1) Gratzel, M. *Prog. Photovoltaics* **2000**, *8*, 171.
- (2) Hagfeldt, A.; Gratzel, M. *Chem. Rev.* **1995**, *95*, 49–68.

- (3) O'Regan, B.; Gratzel, M. *Nature* **1991**, 353, 737–740.
- (4) Sayama, K.; Sugihara, H.; Arakawa, H. *Chem. Mater.* **1998**, 10, 3825–3832.
- (5) Burnside, S.; Moser, J. E.; Brooks, K.; Gratzel, M.; Cahen, D. *J. Phys. Chem. B* **1999**, 103, 9328.
- (6) Chappel, S.; Chen, S. G.; Zaban, A. *Langmuir* **2002**, 18, 3336.
- (7) Zaban, A.; Chen, S. G.; Chappel, S.; Gregg, B. A. *Chem. Commun.* **2000**, 2231.
- (8) Tennakone, K.; Kumara, G. R. R. A.; Kottegoda, I. R. M.; Perera, V. P. S. *Chem. Commun.* **1999**, 15–16.
- (9) Palomares, E.; Clifford, J. N.; Haque, S. A.; Lutz, T.; Durrant, J. R. *J. Am. Chem. Soc.* **2003**, 125, 475.
- (10) Bisquert, J.; Cahen, D.; Hodes, G.; Ruhle, S.; Zaban, A. *J. Phys. Chem. B* **2004**, 108, 8106.
- (11) Cahen, D.; Hodes, G.; Gratzel, M.; Guillemoles, J. F.; Riess, I. *J. Phys. Chem. B* **2000**, 104, 2053.
- (12) Zaban, A.; Meier, A.; Gregg, B. A. *J. Phys. Chem. B* **1997**, 101, 7985.
- (13) Gregg, B. A. *J. Phys. Chem. B* **2003**, 107, 13540.
- (14) Hagfeldt, A.; Bjorksten, U.; Lindquist, S. E. *Sol. Energy Mater. Sol. Cells* **1992**, 27, 293.
- (15) Chappel, S.; Chen, S. G.; Zaban, A. *Langmuir* **2002**, 18, 3336.
- (16) Melnikov, P. S. *The Handbook of Electroplating in Engineering Industry*; Mashinostroeniye: Moscow (Russian); 1991.
- (17) Geul, E. *J. Chem. Educ.* **1993**, 70, 176.
- (18) Choi, Y. K.; Seo, S. S.; Chjo, K. H.; Choi, Q. W.; Park, S. M. *J. Electrochem. Soc.* **1992**, 139, 1803.
- (19) Dutoit, E. C.; Cardon, F. *J. Appl. Electrochem.* **1978**, 8, 247.
- (20) Climent, F.; Capellades, R. *Mater. Lett.* **1994**, 18, 263.
- (21) Cameron, P. J.; Peter, L. M. *J. Phys. Chem. B* **2003**, 107, 14394.
- (22) Bard, A. J.; Faulkner, L. R. *Electrochemical Methods. Fundamentals and Applications*; John Wiley & Sons Inc.: New York, 1980.
- (23) MacDonald, J. R. *Impedance Spectroscopy*; John Wiley & Sons Inc.: New York, 1987.
- (24) Van de Krol, R.; Goossens, A.; Schoonman, J. *J. Electrochem. Soc.* **1997**, 144, 1723.
- (25) Chen, S. G.; Chappel, S.; Diamant, Y.; Zaban, A. *Chem. Mater.* **2001**, 13, 4629.
- (26) Bisquert, J.; Greenshtein, M.; Zaban, A. *ChemPhysChem* **2003**, 4, 859.
- (27) Bisquert, J.; Zaban, A.; Greenshtein, M.; Mora-Sero, I. *J. Am. Chem. Soc.* **2004**, 126, 13550.